Electronic Supplementary Material (ESI) for Dalton Transactions.

Supporting information for

Unexpected alkyl isomerization at the silicon ligand of an unsaturated Rh complex: combined experiment and theory

Niroshani S. Abeynayake,† Nghia Le,† Gabriela Sanchez-Lecuona, Bruno Donnadieu, Charles Edwin Webster,* and Virginia Montiel-Palma*

Department of Chemistry, Mississippi State University, Box 9573, Mississippi State, Mississippi 39762, United States

Emails: ewebster@chemistry.msstate.edu and vmontiel@chemistry.msstate.edu

Table of Contents

1 Experimental details

All experiments were performed under an argon atmosphere using standard Schlenk methods or in an MBraun glove box. Toluene and pentane were dried and purified over MBraun column systems. Benzene-d_6 and toluene-d_8 were passed through a Pasteur pipette containing molecular sieves and basic alumina and then degassed via three freeze–pump–thaw cycles and stored over molecular sieves. Other NMR solvents were used as received. $[RhCl(COD)]_2$[1] and PhP(o-$C_6H_4CH_2Si^iPr_2H)_2$[2] were synthesized according to reported procedures. Nuclear magnetic resonance (NMR) experiments were performed on Bruker Avance 500 MHz and 600 MHz spectrometers operating with frequency, deuterated solvent and temperature indicated in parentheses. Chemical shifts (δ) are reported in parts per million (ppm).

1.1 Isolation of complex [μ-Cl-Rh{κ³(*P,Si,Si*)PPh(*o*-$C_6H_4CH_2Si(^iPr)CH_2CH_2CH_3$)(*o*-$C_6H_4CH_2Si^iPr_2$)]$_2$ (**Rh-3**)

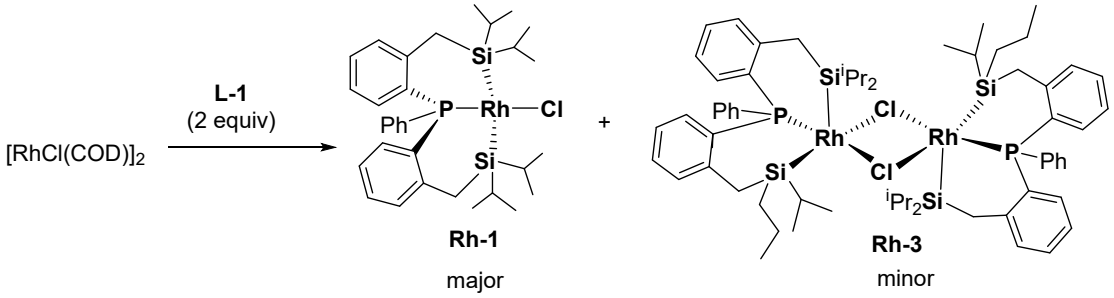

We previously reported the synthesis of complex **Rh-1** from the reaction of $[RhCl(COD)]_2$ (47 mg, 0.097mmol) and **L-1** (100 mg, 0.19 mmol) in toluene.[2] After stirring for 3 h, the solution was concentrated and crystals of **Rh-1** were obtained in 70-73% isolated yield. The remaining mother liquor was dried under vacuum and redissolved in pentane. Orange crystals of complex **Rh-3** were grown. The isolated yield of **Rh-3** was 8-10 mg, corresponding to 13-15% isolated yield (with respect to Rh). Small amounts of **Rh-1** are still present in the recrystallized sample. **^{1}H NMR (600 MHz, C_6D_6, 298 K):** δ 7.04 – 6.84 (m, 21H, CH_{arom}), 6.77 – 6.71 (m, 5H, CH_{arom}), 2.30 – 2.23 (m, 4H, CH_2), 2.14 (dd, J_{HH}= 14.6, J_{HP}= 2.9 Hz, 2H, CH_2), 2.03 (d, J_{HH}= 14.4 Hz, 2H, CH_2), 2.01 – 1.86 (m, 2H,

CH-^{i}Pr), 1.77 – 1.63 (m, 4H, CH-^{i}Pr), 1.61 (d, J_{HH}= 7.2 Hz, 6H, CH_3-^{i}Pr), 1.58-1.51 (m, 4H, CH_2-Propyl), 1.32 (ddd, J_{HH}= 14.6, J_{HH}= 12.7, J_{HP}= 3.9 Hz, 4H, CH_2-Propyl, overlapped), 1.19 (d, J_{HH}= 7.5 Hz, 6H, CH_3-^{i}Pr), 1.13 (d, J_{HH}= 7.3 Hz, 6H, CH_3-^{i}Pr), 1.08 (d, J_{HH}= 7.4 Hz, 6H, CH_3-^{i}Pr), 1.01 (d, J_{HH}= 7.5 Hz, 6H, CH_3-^{i}Pr), 0.99 - 0.96 (overlapped signals: 12H, CH_3-^{i}Pr (6H) and CH_3-Propyl (6H)) ppm. **DEPT $^{13}C\{^{1}H\}$ NMR (150.9 MHz, C_6D_6):** 24.02 (d, J_{CP} = 16.9 Hz, CH_2), 23.07 (d, J_{CP} = 18.3 Hz, CH_2), 21.94 (s, *C*H_3, ^{i}Pr), 20.88 (s, CH_2, *n*-Propyl), 20.59 (s, CH, ^{i}Pr), 20.53 (s, CH, ^{i}Pr), 20.28 (s, CH_3, ^{i}Pr), 20.07 (s, CH_3, ^{i}Pr), 19.87 (s, CH_3, *n*-Propyl), 19.20 (s, CH_3, ^{i}Pr), 18.84 (s, CH_2, *n*-Propyl), 18.51 (s, CH_3, ^{i}Pr), 18.41 (s, CH_3, *n*-Propyl) ppm. **$^{31}P\{^{1}H\}$ NMR (202.46 MHz, C_6D_6):** 31.5 (d, J_{PRh}= 145.7 Hz) ppm. Anal. Calcd. For $C_{32}H_{45}RhClPSi_2$: C, 58.66%; H, 6.92%. Found: C, 57.23%; H, 5.90%. The deviation in the C and H values for microanalysis maybe due to small decomposition of the **Rh-3** sample as the microanalyses we carried out. The sample also contains isomer **Rh-1** with the same formula.

1.2 Formation of [μ-Cl-Rh{κ^3(*P,Si,C*)PPh(o-$C_6H_4CH_2Si^{i}PrO$ $Si^{i}Pr_2CH$-o-C_6H_4)}]$_2$ (**Rh-4**) in the presence of adventitious water

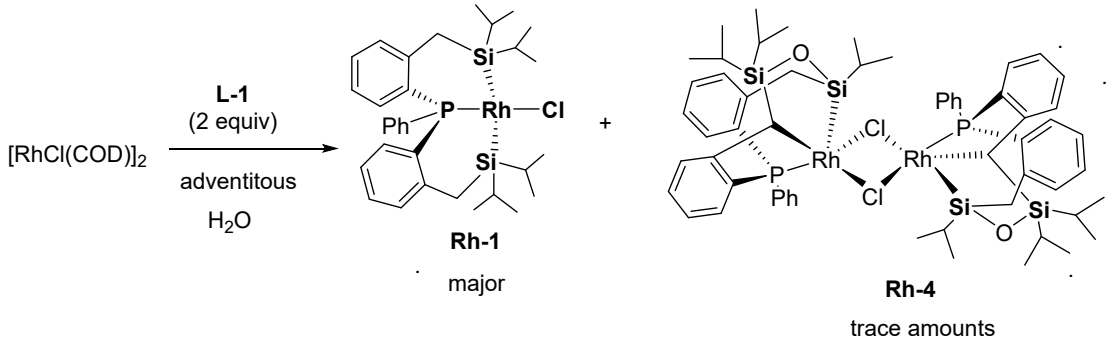

Following the procedure described in Section 1.1 above, 47 mg (0.097mmol) of $[RhCl(COD)]_2$ and 100 mg of **L-1** (0.19 mmol) in 2 mL of not-freshly dried toluene (with trace amounts of water) rendered crystals of **Rh-1** which were subsequently removed. The volatiles were dried under vacuum and redissolved in pentane from which yellow crystals of complex **Rh-4** were obtained. The crystals were suitable for X-ray diffraction analysis. Isolated yield 6 mg, 5%. **^{1}H NMR (500 MHz, C_6D_6, 298 K):** δ 7.48 – 7.37 (m, 5H, CH_{arom}), 7.13 – 6.97 (m, 31H, CH_{arom}), 2.58 – 2.24 (m, 4H, CH_2), 1.80 (sept, J_{HH} = 7.1 Hz, 4H, CH-^{i}Pr), 1.49 (d, J_{HH} = 7.6 Hz, 6H, CH_3-^{i}Pr), 1.41 (d, J_{HH} = 6.8 Hz, 6H, CH_3-^{i}Pr), 0.84 (d, J_{HH} = 7.5 Hz, 12H, CH_3-^{i}Pr), 0.60 (d, J_{HH} = 7.4 Hz, 6H, CH_3-^{i}Pr), 0.38 (d, J_{HH} = 7.5

Hz, 6H, CH_3-^{i}Pr), 0.10 – 0.02 (m, 2H, CH-^{i}Pr), ppm. **$^{31}P\{^1H\}$ NMR (202.46 MHz, C_6D_6):** 49.04 (d, J_{PRh} = 164.0 Hz) ppm. Attempts to generate this complex from stoichiometric water addition to either **Rh-1** or **Rh-3** were not successful and instead other unidentified compounds were formed. Attempts at deliberate addition of drops of water to the synthesis reaction did not further improve the yield but only the same unidentified compounds were formed and **Rh-4** in approximately the same yield. Fresh rigorously dried toluene did not lead to the observation of **Rh-4**. Complex **Rh-4** is thus generated in the presence of adventitious water. We were unable to obtain successful microanalysis of this complex as the separation of this complex from the major product **Rh-1** proved impossible in our hands.

The X-ray diffraction structure (**Figure 1** in the main text) discloses a symmetric dichloro-bridged dimetallic species with modified ligands. The coordination geometry around each Rh center can be described as distorted square pyramidal. Each pentacoordinated Rh(III) metal center is bound to the phosphorous atom, a benzylic carbon and only one silicon atom of the ligand. The new Rh-C bonds result from intramolecular benzylic C-H activation of the formerly methylene carbon. The Si atom bound to Rh bears only one isopropyl substituent whereas the other silicon atom, alfa to the cyclometalated C, no longer binds to Rh but instead to O, forming part of a Si-O-Si motif. The bond lengths and angles are within the expected ranges of other siloxanes.[3-5] The formation of Si-O-Si complexes has been reported by several authors (**Chart S1**). For example, oxidation of the Pt disilene complex [$(PR_3)_2$Pt-η^2(Mes_2Si=SiMes_2)][6] by West and coworkers, and dehydrogenative condensation on [(dmpe)Pt($SiHPh_2)_2$] upon reaction with water by Osakada and coworkers,[7] rendered four-membered Si-O-Si platinacycle units. Ozerov and coworkers reported Si-O-Si motifs bridiging two Pt units from reaction of adventitious water with three-coordinate cationic Pt-PSiP,[8] in a variation of Milstein's saturated Cl-Pt-PSiP system, in which the rearrangement of a pincer silanol Pt complex in the presence of water and a non-nucleophilic base led to a binuclear complex bearing a Si-O-Si-O motif bridging two Pt centers.[9] Adventitious water also reacts with a terminal silylene[10] or σ(Si-H) complexes[11] forming bimetallic Si-O-Si bridges spanning two Ir or Rh centers as reported by Tilley and coworkers (**Chart S1**).

In our case, stoichiometric addition of water to either **Rh-1** or **Rh-3** does not lead to the formation of **Rh-4** but instead, other unidentified products are generated. We thus propose that complex **Rh-4** is also formed during the metalation process from the reaction of one of the intermediate species with adventitious water.

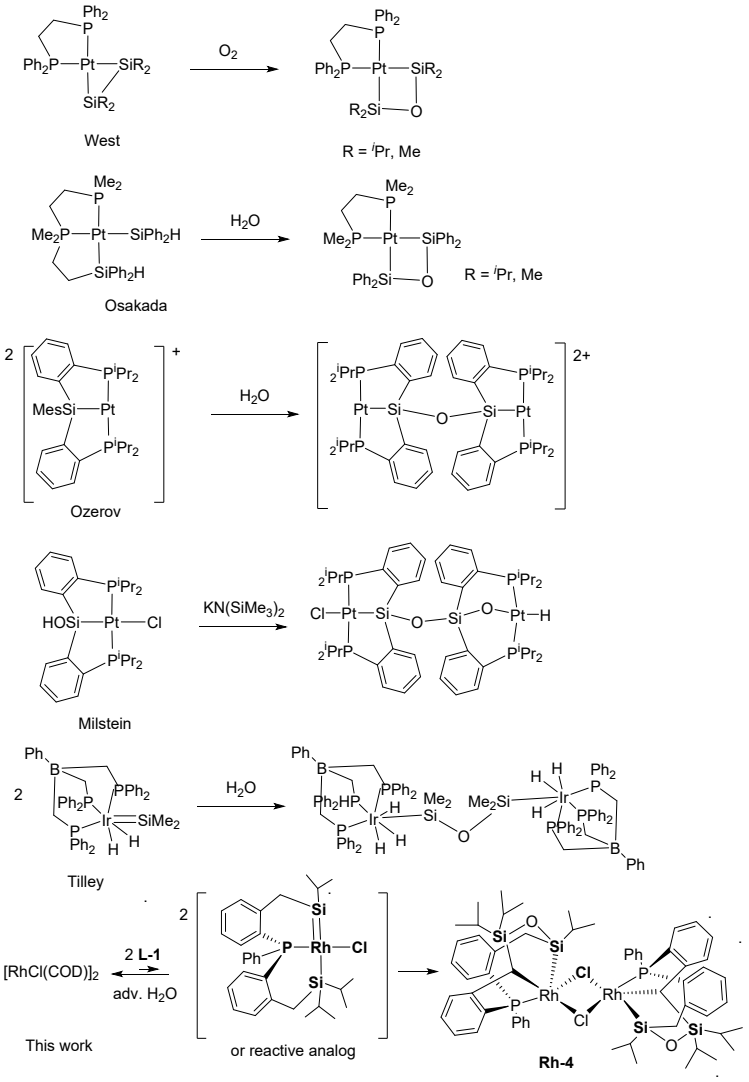

Chart S1. Some examples of the formation of complexes containing Si-O-Si motifs.

2 NMR spectra

2.1 NMR spectra of complex **Rh-3**

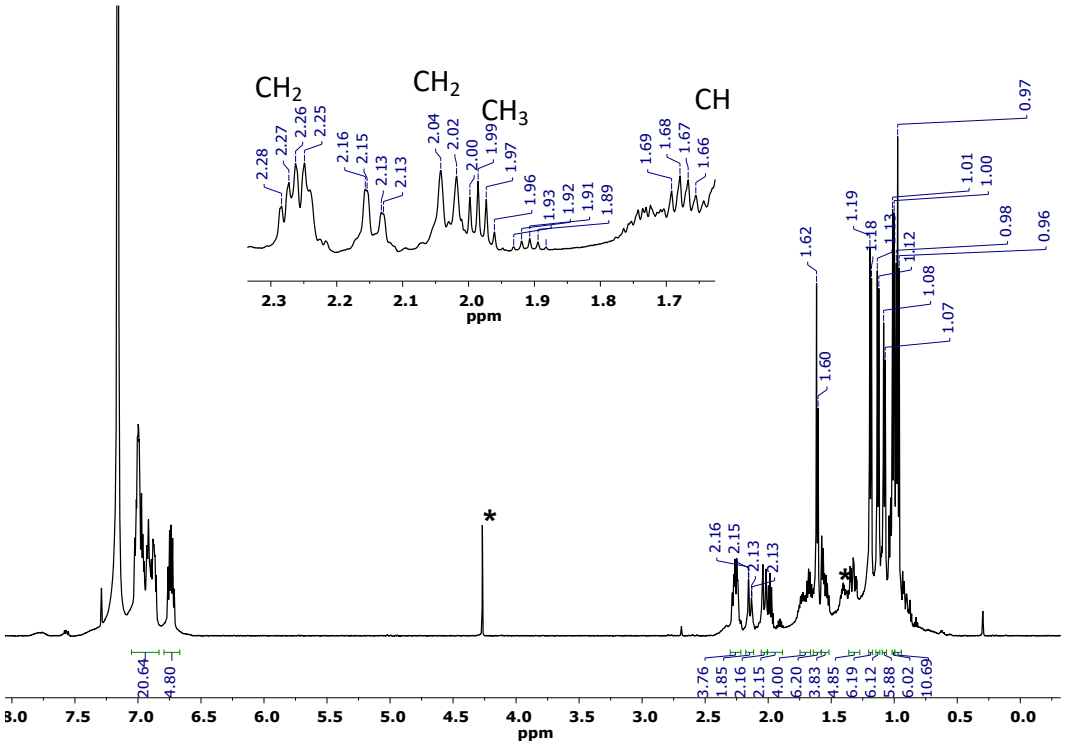

Figure S1. ^{1}H NMR spectrum (600 MHz, C_6D_6, 298 K) of **Rh-3** (*=DCM and pentane remaining from synthesis). Small amounts of **Rh-1** were present in the sample.

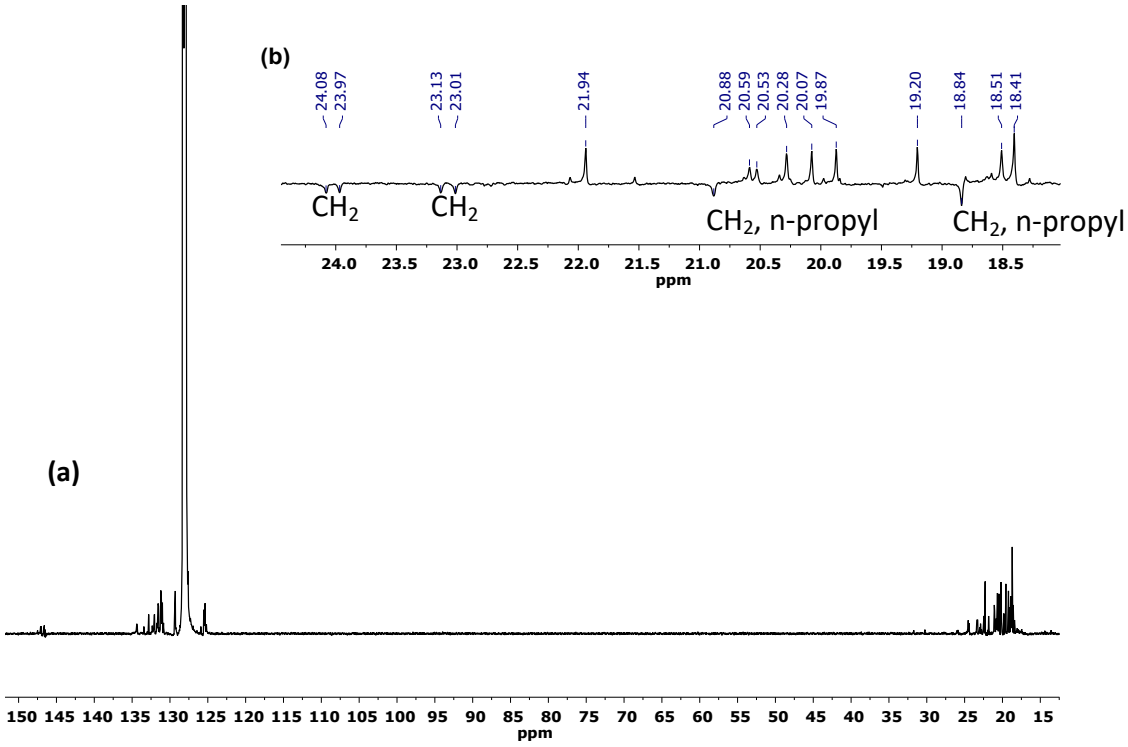

Figure S2. (a) $^{13}C\{^{1}H\}$ NMR spectrum (150.9MHz, C_6D_6, 298 K) of **Rh-3.** (b) DEPT$^{13}C\{^{1}H\}$ NMR spectrum (150.9MHz, C_6D_6, 298 K) of **Rh-3.** Small amounts of **Rh-1** were present in the sample.

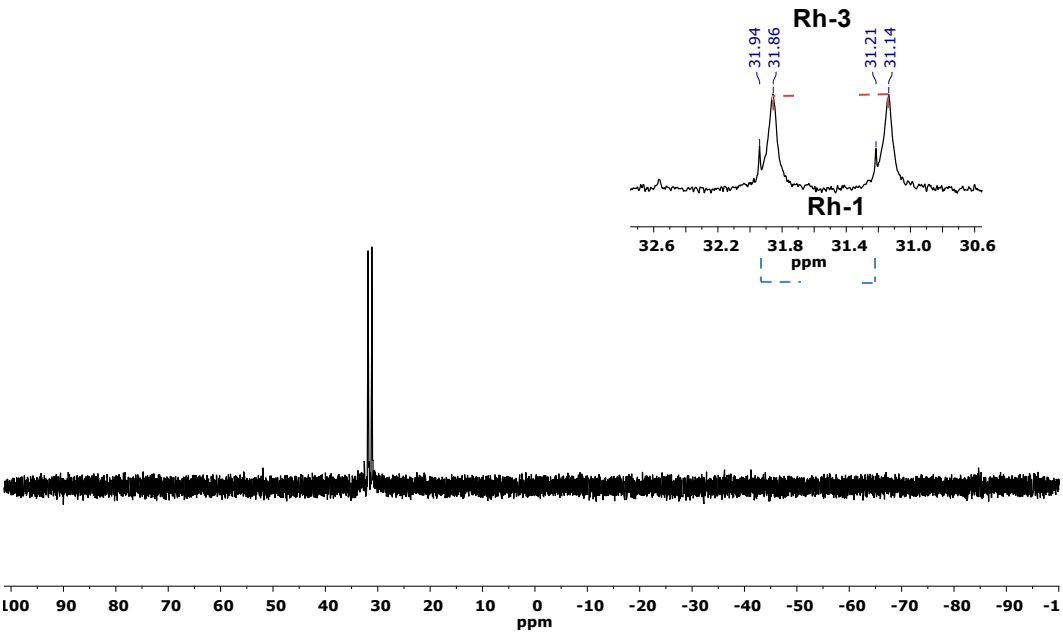

Figure S3. $^{31}P\{^{1}H\}$ NMR spectrum (202.46 MHz, C_6D_6, 298 K) of **Rh-3.** Small amounts of **Rh-1** were present in the sample.

2.2 NMR spectra for **Rh-4**

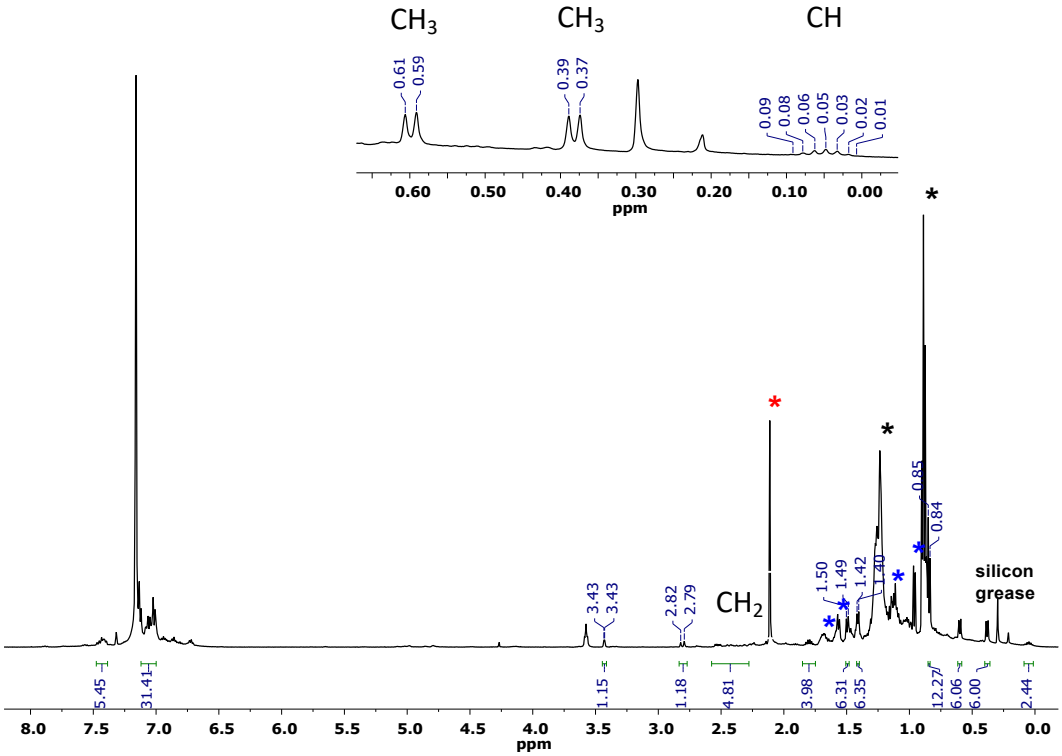

Figure S4.[1]H NMR spectrum (500 MHz, C_6D_6, 298 K) of **Rh-4** (*=pentane, *=Toluene, *=**Rh-1**). This complex is not isolated pure but **Rh-1** co-crystallizes with it.

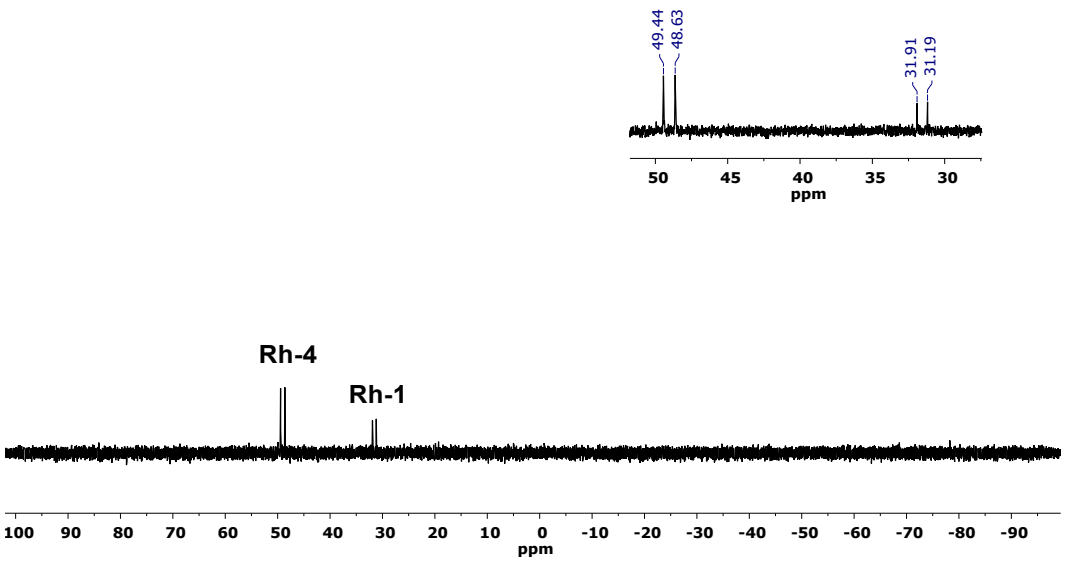

Figure S5. $^{31}P\{^{1}H\}$ NMR spectrum (202.46 MHz, C_6D_6, 278 K) of **Rh-4** showing also the presence of **Rh-1.**

3 X-ray diffraction analysis data for the complexes

3.1 X-ray diffraction data of complex **Rh-3** (CCDC 2133159)

Crystal Structure Report for A_VM_018

An orange prism single crystal of $C_{32}H_{45}ClPRhSi_2$, approximate dimensions (0.110 x 0.176 x 0.234) mm^3, was selected for the X-ray crystallographic analysis and mounted on a cryo-loop using an oil cryo-protectant. The X-ray intensity data was measured at low temperature (T = 100K), using a three circles goniometer Kappa geometry with a fixed Kappa angle at = 54.74 deg Bruker AXS D8 Venture, equipped with a Photon 100 CMOS active pixel sensor detector. A monochromatized Mo X-ray radiation (λ = 0.71073 Å) was selected for the measurement. Frames were integrated with the Bruker SAINT using a narrow-frame algorithm.[12,13] The integration of the data using an orthorhombic unit cell yielded a total of 99234reflections to a maximum θ angle of 32.03° (0.67 Å resolution), of which 10715 were independent (average redundancy 9.261, completeness = 99.4%, R_{int} = 4.18%, R_{sig} = 2.39%) and 8971 (83.72%) were greater than 2σ (F^2). The final cell constants of a = 19.691(7) Å, b = 15.587(7) Å, c = 20.196(9) Å, volume = 6199. (4) $Å^3$, are based upon the refinement of the XYZ-centroids of 1261 reflections above 20 σ (I) with 4.526° < 2θ < 43.11°. Data were corrected for absorption effects using the multi-Scan method implemented in the software (SADABS). The ratio of minimum to maximum apparent transmission was 0.874. The calculated minimum and maximum transmission coefficients (based on crystal size) are 0.8370 and 0.9180. The structure was solved in an orthorhombic unit cell, Space Group: P b c a, with Z = 8 for the formula unit, $C_{32}H_{45}ClPRhSi_2$ using the Bruker SHELXT Software.[14] The asymmetric unit was built on half of molecule, the entire model being generated by an inversion center. Refinement of the structure was carried out by least squares procedures on weighted F^2 values using the SHELXTL-2018/3[15] included in the APEX3 v2018, 7.0, AXS Bruker program.[16] All hydrogen atoms were localized on difference Fourier maps but then introduced in the refinement as fixed contributors in idealized geometry with an isotropic thermal parameter fixed at 20% higher than those carbons atoms they were connected. The final anisotropic full-matrix least-squares refinement on F^2 with 341 variables converged at R1 = 3.16%, for the observed data and wR2 = 8.94% for all data. The goodness-of-fit: GOF was 1.062. The largest peak in the final

difference electron density synthesis was 1.004 $e^-/Å^3$ and the largest hole was -0.595 $e^-/Å^3$ with an RMS deviation of 0.118 $e^-/Å^3$. On the basis of the final model, the calculated density was 1.404 g/cm^3 and F (000), 2736 e^-. Graphics were performed using softwares: Mercury V.4.2.0: (https://www.ccdc.cam.ac.uk/) and POV-Ray v 3.7: (The Persistence of Vision Raytracer, high quality, Free Software tool).

Molecule's view:

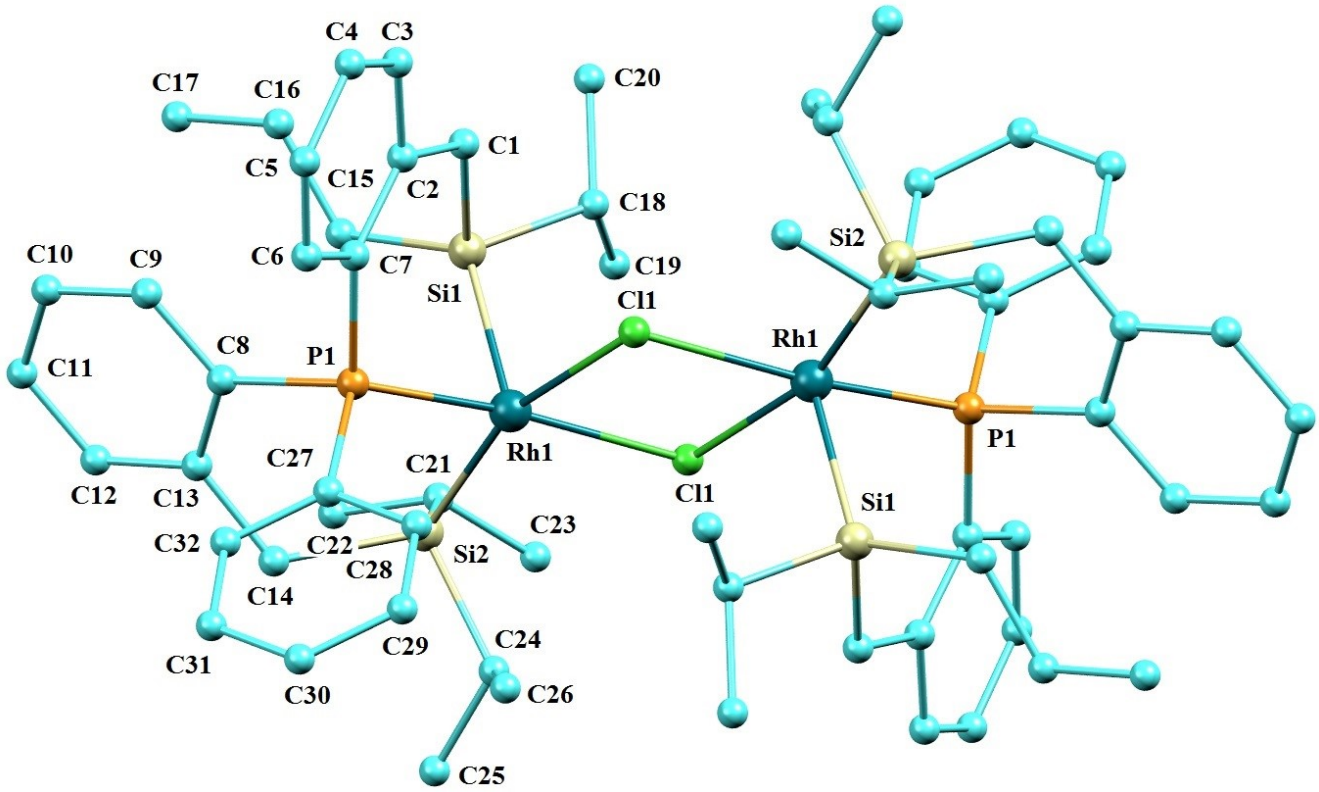

Figure S6. Asymmetric unit view of complex **Rh-3**

Table S1. ***Sample and crystal data for A_VM_018.***

Identification code	A_VM_018	
Chemical formula	$C_{64}H_{90}Cl_2P_2Rh_2Si_4$	
Formula weight	1310.37 g/mol	
Temperature	100(2) K	
Wavelength	0.71073 Å	
Crystal size	(0.110 x 0.176 x 0.234) mm^3	
Crystal system	orthorhombic	
Space group	P b c a	
Unit cell dimensions	a = 19.691(7) Å	α = 90°
	b = 15.587(7) Å	β = 90°
	c = 20.196(9) Å	γ = 90°
Volume	6199.(4) $Å^3$	
Z	4	
Density (calculated)	1.404 g/cm^3	
Absorption coefficient	0.787 mm^{-1}	
F(000)	2736	

Table S2. ***Data collection and structure refinement for A_VM_018.***

Theta range for data collection	2.27 to 32.03°
Index ranges	-28<=h<=29, -23<=k<=23, -30<=l<=30
Reflections collected	99234
Independent reflections	10715 [R(int) = 0.0418]
Coverage of independent	99.4%
Absorption correction	Multi-Scan
Max. and min. transmission	0.9180 and 0.8370
Structure solution technique	direct methods
Structure solution program	XT, VERSION 2014/5
Refinement method	Full-matrix least-squares on F^2
Refinement program	SHELXL-2018/3 (Sheldrick, 2018)
Function minimized	$\Sigma\, w(F_o^2 - F_c^2)^2$
Data / restraints / parameters	10715 / 0 / 341
Goodness-of-fit on F^2	1.062
Δ/σ_{max}	0.002
Final R indices	8971 data; I>2σ(I) R1 = 0.0316, wR2 = 0.0810
	all data R1 = 0.0426, wR2 = 0.0894
Weighting scheme	$w=1/[\sigma^2(F_o^2)+(0.0400P)^2+6.5530P]$
Largest diff. peak and hole	1.004 and -0.595 eÅ^{-3}
R.M.S. deviation from mean	0.118 eÅ^{-3}

Table S3. ***Atomic coordinates and equivalent isotropic atomic displacement parameters (Å²) for A_VM_018.***

U(eq) is defined as one third of the trace of the orthogonalized U_{ij} tensor.

	x/a	y/b	z/c	U(eq)
Rh1	0.45055(2)	0.41638(2)	0.04764(2)	0.01719(4)
Cl1	0.44800(2)	0.48012(3)	0.93831(2)	0.02300(8)
P1	0.44817(2)	0.37515(3)	0.15226(2)	0.01856(8)
Si1	0.50732(2)	0.28928(3)	0.02879(2)	0.02126(9)
Si2	0.34188(2)	0.36394(3)	0.03117(2)	0.02173(9)
C1	0.58732(9)	0.30342(12)	0.08089(9)	0.0264(3)
C2	0.58850(9)	0.33206(11)	0.15225(9)	0.0235(3)
C3	0.65177(10)	0.32641(13)	0.18435(10)	0.0298(4)
C4	0.66153(11)	0.35543(14)	0.24836(11)	0.0352(4)

	x/a	y/b	z/c	U(eq)
C5	0.60768(11)	0.39087(13)	0.28294(10)	0.0332(4)
C6	0.54410(10)	0.39592(12)	0.25301(9)	0.0268(3)
C7	0.53352(9)	0.36667(11)	0.18831(8)	0.0218(3)
C8	0.40537(9)	0.27585(11)	0.17634(8)	0.0226(3)
C9	0.43817(10)	0.21538(12)	0.21649(9)	0.0265(3)
C10	0.40592(11)	0.13917(13)	0.23465(9)	0.0315(4)
C11	0.34066(11)	0.12323(13)	0.21257(10)	0.0321(4)
C12	0.30740(10)	0.18270(12)	0.17280(9)	0.0280(3)
C13	0.33853(9)	0.25980(12)	0.15358(8)	0.0240(3)
C14	0.30074(9)	0.32292(12)	0.11117(9)	0.0257(3)
C15	0.46938(11)	0.17857(12)	0.04377(9)	0.0283(4)
C16	0.51724(13)	0.11500(14)	0.07857(12)	0.0385(5)
C17	0.48305(18)	0.02811(16)	0.09017(15)	0.0555(7)
C18	0.54311(10)	0.29043(13)	0.94067(9)	0.0282(4)
C19	0.49370(11)	0.27037(14)	0.88502(10)	0.0345(4)
C20	0.60428(12)	0.22884(16)	0.93423(12)	0.0411(5)
C21	0.33160(10)	0.28218(13)	0.96069(9)	0.0289(4)
C22	0.28627(12)	0.20628(14)	0.97688(11)	0.0372(4)
C23	0.31030(12)	0.32268(15)	0.89469(10)	0.0375(5)
C24	0.28953(9)	0.46452(12)	0.01267(10)	0.0296(4)
C25	0.21220(11)	0.44923(15)	0.01420(13)	0.0412(5)
C26	0.30864(12)	0.53710(14)	0.06035(12)	0.0374(4)
C27	0.40620(9)	0.45567(12)	0.20498(8)	0.0236(3)
C28	0.42165(10)	0.54257(12)	0.19531(9)	0.0267(3)
C29	0.38971(11)	0.60564(13)	0.23302(10)	0.0324(4)
C30	0.34247(12)	0.58237(15)	0.28097(12)	0.0405(5)
C31	0.32738(13)	0.49671(16)	0.29157(12)	0.0438(5)
C32	0.35907(11)	0.43316(14)	0.25358(10)	0.0342(4)

Table S4. ***Bond lengths (Å) for A_VM_018.***

Rh1-P1	2.2088(10)	Rh1-Si1	2.3064(9)
Rh1-Si2	2.3147(9)	Rh1-Cl1	2.4217(10)
Rh1-Cl1#1	2.5832(8)	P1-C8	1.8282(18)
P1-C7	1.8364(18)	P1-C27	1.8416(18)
Si1-C15	1.905(2)	Si1-C1	1.9071(19)
Si1-C18	1.914(2)	Si2-C24	1.913(2)
Si2-C14	1.9172(19)	Si2-C21	1.921(2)
C1-C2	1.509(3)	C1-H1A1	0.99
C1-H1A2	0.99	C2-C3	1.407(2)
C2-C7	1.412(3)	C3-C4	1.383(3)
C3-H3A	0.95	C4-C5	1.385(3)
C4-H4A	0.95	C5-C6	1.392(3)
C5-H5A	0.95	C6-C7	1.400(2)
C6-H6A	0.95	C8-C9	1.401(2)
C8-C13	1.416(2)	C9-C10	1.396(3)
C9-H9A	0.95	C10-C11	1.383(3)
C10-H10A	0.95	C11-C12	1.390(3)
C11-H11A	0.95	C12-C13	1.404(3)
C12-H12A	0.95	C13-C14	1.502(3)
C14-H14A	0.99	C14-H14B	0.99
C15-C16	1.538(3)	C15-H15A	0.99
C15-H15B	0.99	C16-C17	1.531(3)
C16-H16A	0.99	C16-H16B	0.99
C17-H17A	0.98	C17-H17B	0.98
C17-H17C	0.98	C18-C19	1.519(3)
C18-C20	1.546(3)	C18-H18A	1.0
C19-H19A	0.98	C19-H19B	0.98
C19-H19C	0.98	C20-H20A	0.98
C20-H20B	0.98	C20-H20C	0.98
C21-C22	1.518(3)	C21-C23	1.533(3)
C21-H21A	1.0	C22-H22A	0.98
C22-H22B	0.98	C22-H22C	0.98
C23-H23A	0.98	C23-H23B	0.98
C23-H23C	0.98	C24-C26	1.533(3)
C24-C25	1.542(3)	C24-H24A	1.0

C25-H25A	0.98	C25-H25B	0.98
C25-H25C	0.98	C26-H26A	0.98
C26-H26B	0.98	C26-H26C	0.98
C27-C32	1.396(3)	C27-C28	1.402(3)
C28-C29	1.394(3)	C28-H28A	0.95
C29-C30	1.391(3)	C29-H29A	0.95
C30-C31	1.385(3)	C30-H30A	0.95
C31-C32	1.400(3)	C31-H31A	0.95
C32-H32A	0.95		

Symmetry transformations used to generate equivalent atoms:

#1 -x+1, -y+1, -z

Table S5. *Bond angles (°) for A_VM_018.*

P1-Rh1-Si1	85.31(2)	P1-Rh1-Si2	90.864(18)
Si1-Rh1-Si2	96.95(3)	P1-Rh1-Cl1	172.308(17)
Si1-Rh1-Cl1	102.23(2)	Si2-Rh1-Cl1	89.696(19)
P1-Rh1-Cl1#1	95.343(19)	Si1-Rh1-Cl1#1	100.36(3)
Si2-Rh1-Cl1#1	162.021(18)	Cl1-Rh1-Cl1#1	81.95(2)
Rh1-Cl1-Rh1#1	98.05(2)	C8-P1-C7	104.80(8)
C8-P1-C27	102.49(8)	C7-P1-C27	103.33(8)
C8-P1-Rh1	120.70(6)	C7-P1-Rh1	112.38(6)
C27-P1-Rh1	111.36(6)	C15-Si1-C1	109.95(9)
C15-Si1-C18	107.50(9)	C1-Si1-C18	101.99(9)
C15-Si1-Rh1	124.19(7)	C1-Si1-Rh1	102.12(6)
C18-Si1-Rh1	108.90(7)	C24-Si2-C14	102.14(9)
C24-Si2-C21	110.00(9)	C14-Si2-C21	111.02(9)
C24-Si2-Rh1	103.70(7)	C14-Si2-Rh1	112.79(6)
C21-Si2-Rh1	115.98(7)	C2-C1-Si1	125.02(13)
C2-C1-H1A1	106.1	Si1-C1-H1A1	106.1
C2-C1-H1A2	106.1	Si1-C1-H1A2	106.1
H1A1-C1-H1A2	106.3	C3-C2-C7	117.71(16)
C3-C2-C1	115.80(16)	C7-C2-C1	126.43(15)
C4-C3-C2	122.23(19)	C4-C3-H3A	118.9
C2-C3-H3A	118.9	C3-C4-C5	119.70(18)
C3-C4-H4A	120.1	C5-C4-H4A	120.1
C4-C5-C6	119.48(18)	C4-C5-H5A	120.3

C6-C5-H5A	120.3	C5-C6-C7	121.39(18)
C5-C6-H6A	119.3	C7-C6-H6A	119.3
C6-C7-C2	119.47(16)	C6-C7-P1	118.88(14)
C2-C7-P1	121.65(13)	C9-C8-C13	119.82(16)
C9-C8-P1	120.73(14)	C13-C8-P1	119.45(13)
C10-C9-C8	120.98(18)	C10-C9-H9A	119.5
C8-C9-H9A	119.5	C11-C10-C9	119.41(18)
C11-C10-H10A	120.3	C9-C10-H10A	120.3
C10-C11-C12	120.28(17)	C10-C11-H11A	119.9
C12-C11-H11A	119.9	C11-C12-C13	121.65(18)
C11-C12-H12A	119.2	C13-C12-H12A	119.2
C12-C13-C8	117.86(16)	C12-C13-C14	120.14(16)
C8-C13-C14	121.99(15)	C13-C14-Si2	119.32(13)
C13-C14-H14A	107.5	Si2-C14-H14A	107.5
C13-C14-H14B	107.5	Si2-C14-H14B	107.5
H14A-C14-H14B	107.0	C16-C15-Si1	114.58(15)
C16-C15-H15A	108.6	Si1-C15-H15A	108.6
C16-C15-H15B	108.6	Si1-C15-H15B	108.6
H15A-C15-H15B	107.6	C17-C16-C15	111.7(2)
C17-C16-H16A	109.3	C15-C16-H16A	109.3
C17-C16-H16B	109.3	C15-C16-H16B	109.3
H16A-C16-H16B	107.9	C16-C17-H17A	109.5
C16-C17-H17B	109.5	H17A-C17-H17B	109.5
C16-C17-H17C	109.5	H17A-C17-H17C	109.5
H17B-C17-H17C	109.5	C19-C18-C20	107.99(17)
C19-C18-Si1	116.75(14)	C20-C18-Si1	111.06(14)
C19-C18-H18A	106.8	C20-C18-H18A	106.8
Si1-C18-H18A	106.8	C18-C19-H19A	109.5
C18-C19-H19B	109.5	H19A-C19-H19B	109.5
C18-C19-H19C	109.5	H19A-C19-H19C	109.5
H19B-C19-H19C	109.5	C18-C20-H20A	109.5
C18-C20-H20B	109.5	H20A-C20-H20B	109.5
C18-C20-H20C	109.5	H20A-C20-H20C	109.5
H20B-C20-H20C	109.5	C22-C21-C23	110.33(16)
C22-C21-Si2	114.79(14)	C23-C21-Si2	113.56(15)
C22-C21-H21A	105.8	C23-C21-H21A	105.8
Si2-C21-H21A	105.8	C21-C22-H22A	109.5

C21-C22-H22B	109.5	H22A-C22-H22B	109.5
C21-C22-H22C	109.5	H22A-C22-H22C	109.5
H22B-C22-H22C	109.5	C21-C23-H23A	109.5
C21-C23-H23B	109.5	H23A-C23-H23B	109.5
C21-C23-H23C	109.5	H23A-C23-H23C	109.5
H23B-C23-H23C	109.5	C26-C24-C25	110.13(19)
C26-C24-Si2	110.47(14)	C25-C24-Si2	113.68(14)
C26-C24-H24A	107.4	C25-C24-H24A	107.4
Si2-C24-H24A	107.4	C24-C25-H25A	109.5
C24-C25-H25B	109.5	H25A-C25-H25B	109.5
C24-C25-H25C	109.5	H25A-C25-H25C	109.5
H25B-C25-H25C	109.5	C24-C26-H26A	109.5
C24-C26-H26B	109.5	H26A-C26-H26B	109.5
C24-C26-H26C	109.5	H26A-C26-H26C	109.5
H26B-C26-H26C	109.5	C32-C27-C28	119.02(17)
C32-C27-P1	122.25(15)	C28-C27-P1	118.72(13)
C29-C28-C27	120.50(18)	C29-C28-H28A	119.7
C27-C28-H28A	119.7	C30-C29-C28	119.9(2)
C30-C29-H29A	120.1	C28-C29-H29A	120.1
C31-C30-C29	120.17(19)	C31-C30-H30A	119.9
C29-C30-H30A	119.9	C30-C31-C32	120.1(2)
C30-C31-H31A	119.9	C32-C31-H31A	119.9
C27-C32-C31	120.3(2)	C27-C32-H32A	119.9
C31-C32-H32A	119.9		

Symmetry transformations used to generate equivalent atoms:

#1 -x+1, -y+1, -z

3.2 X-ray diffraction data of complex **Rh-4** (CCDC 2133161)

Crystal Structure Report for A_VM_005_bi

A yellow light crystal prism like $C_{32}H_{40}ClOPRhSi_2$, approximate dimensions (0.107 x 0.173 x 0.303) mm^3, was selected for the X-ray crystallographic analysis and mounted on a cryoloop using an oil cryoprotectant. The X-ray intensity data was measured at low temperature (T = 100K), using a three circles goniometer Kappa geometry with a fixed Kappa angle at = 54.74 deg Bruker AXS D8 Venture, equipped with a Photon 100 CMOS active pixel sensor detector. A monochromatized Copper X-ray radiation was used. Frames were integrated with the Bruker SAINT software using a narrow-frame algorithm.[12,13] The integration of the data using a triclinic unit cell yielded a total of 24271 reflections to a maximum θ angle of 72.57° (0.81 Å resolution), of which 24271 were independent (average redundancy 1.000, completeness = 98.0%, R_{sig} = 7.31%) and 21580 (88.91%) were greater than 2σ (F^2). The final cell constants of a =9.844(5) Å, b = 11.815(7) Å, c = 13.809(8) Å, α = 102.799(15) °, β = 95.00(2) °, γ = 97.929(16) °, volume = 1539.6(15) $Å^3$, are based upon the refinement of the XYZ-centroids of 1331 reflections above 20 σ (I) with 6.613° < 2θ <51.84°. Data were corrected for absorption effects using the multi-Scan method (SADABS). The calculated minimum and maximum transmission coefficients (based on crystal size) are 0.2360 and 0.5340. The structure was solved in a triclinic unit cell using the Bruker SHELXT Software Package,[14] using the centrosymmetric space group P -1, with Z = 2 for the formula unit, $C_{32}H_{40}ClOPRhSi_2$. Refinement of the structure was carried out by least squares procedures on weighted F^2 values using the SHELXTL-2018/3[15] included in the APEX3 v2018, 7.0, AXS Bruker program.[16] Hydrogen atoms were localized on difference Fourier maps but then introduced in the refinement as fixed contributors in idealized geometry with an isotropic thermal parameter fixed at 20 % higher than those carbons atoms they were connected. A molecule of solvent: Benzene was found crystallized with the complex. Some iPr groups were found to be statistically disordered and were anisotropically refined with a ratio of occupancy equal to 52/4%. Restraints were added on interatomic lengths and angles. Finally, a non-merohedral twinning was depicted using the software Cell_now integrated in APEX3 v2018, 7.0. The final anisotropic full-matrix

least-squares refinement on F^2 with409 variables converged at R1 = 4.30%, for the observed data and wR2 = 11.29% for all data. The goodness-of-fit: GOF was 1.027. The largest peak in the final difference electron density synthesis was 0.880 $e^-/Å^3$ and the largest whole was-1.154 $e^-/Å^3$ with an RMS deviation of 0.095 $e^-/Å^3$. On the basis of the final model, the calculated density was 1.437 g/cm^3 and F (000), 690 e^-. Cif file was formatted using CIF format: Hall, S. R.; McMahon, B. International Tables for Crystallography Volume G: Definition and exchange of crystallographic data. Dordrecht: Springer 2005.

Crystal's views:

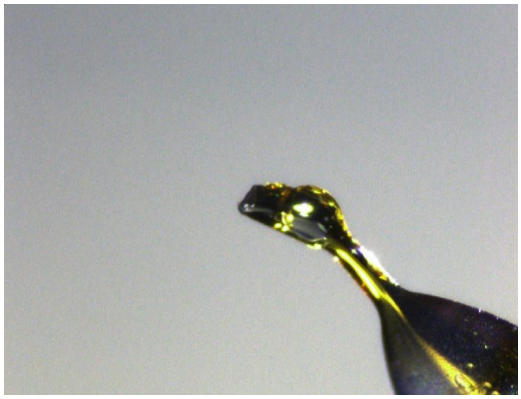
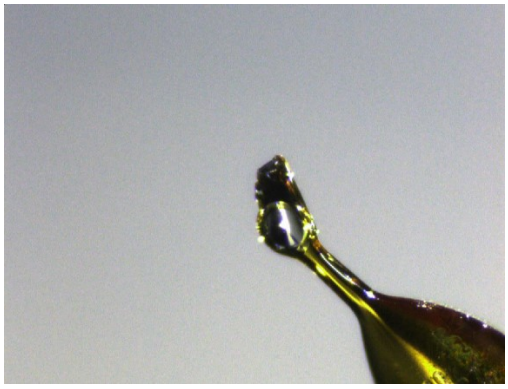
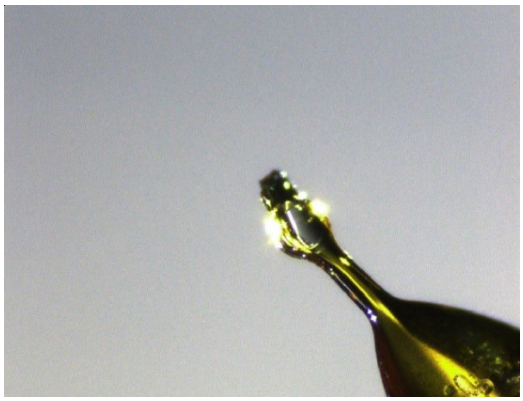
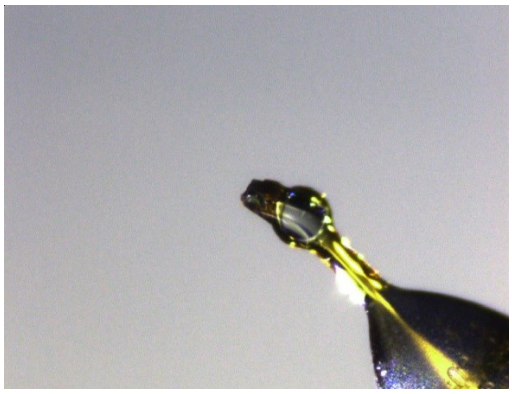

Twin Peaks:

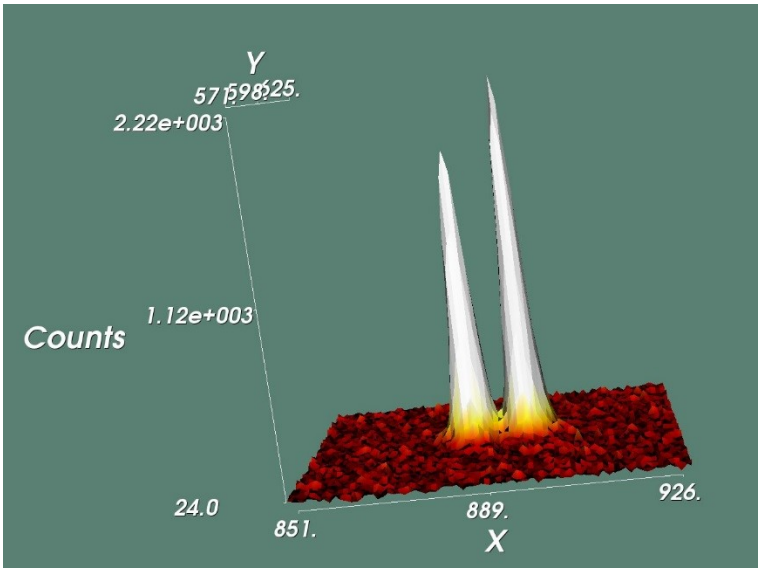

Asymmetric unit's view:

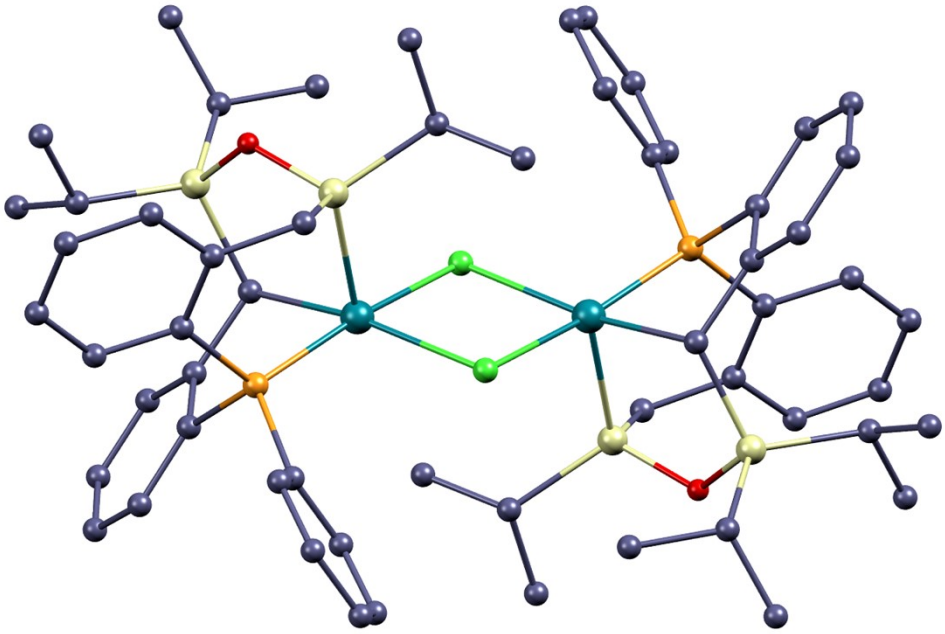

Figure S7. Asymmetric unit view of complex **Rh-4**

Table S6. ***Sample and crystal data for Cu_A_VM_005_bi.***

Identification code	Cu_A_VM_005_bi	
Chemical formula	$C_{32}H_{40}ClOPRhSi_2$	
Formula weight	666.15 g/mol	
Temperature	100(2) K	
Wavelength	1.54178 Å	
Crystal size	(0.107 x 0.173 x 0.303) mm^3	
Crystal system	triclinic	
Space group	P -1	
Unit cell dimensions	a = 9.844(5) Å	α = 102.799(15)°
	b = 11.815(7) Å	β = 95.00(2)°
	c = 13.809(8) Å	γ = 97.929(16)°
Volume	1539.6(15) $Å^3$	
Z	2	
Density (calculated)	1.437 g/cm^3	
Absorption coefficient	6.699 mm^{-1}	
F(000)	690	

Table S7. ***Data collection and structure refinement for Cu_A_VM_005_bi.***

Theta range for data collection	3.31 to 72.57°	
Index ranges	-12<=h<=12, -14<=k<=14, -17<=l<=17	
Reflections collected	24271	
Coverage of independent reflections	98.0%	
Max. and min. transmission	0.5340 and 0.2360	
Structure solution technique	direct methods	
Structure solution program	XT, VERSION 2014/5	
Refinement method	Full-matrix least-squares on F^2	
Refinement program	SHELXL-2018/3 (Sheldrick, 2018)	
Function minimized	$\Sigma\, w(F_o^2 - F_c^2)^2$	
Data / restraints / parameters	24271 / 180 / 409	
Goodness-of-fit on F^2	1.027	
Δ/σ_{max}	0.001	
Final R indices	21580 data; I>2σ(I)	R1 = 0.0430, wR2 = 0.1067
	all data	R1 = 0.0519, wR2 = 0.1129
Weighting scheme	$w=1/[\sigma^2(F_o^2)+(0.0413P)^2+1.6201P]$ where $P=(F_o^2+2F_c^2)/3$	
Largest diff. peak and hole	0.880 and -1.154 eÅ^{-3}	
R.M.S. deviation from mean	0.095 eÅ^{-3}	

Table S8. ***Atomic coordinates and equivalent isotropic atomic displacement parameters (Å²) for Cu_A_VM_005_bi.***

U(eq) is defined as one third of the trace of the orthogonalized U_{ij} tensor.

	x/a	y/b	z/c	U(eq)
Rh1	0.57889(3)	0.43011(3)	0.89749(3)	0.02882(12)
Cl1	0.63931(12)	0.60381(12)	0.03314(11)	0.0551(4)
P1	0.55558(10)	0.25819(9)	0.78926(8)	0.0212(2)
Si1	0.50046(12)	0.51019(11)	0.77302(11)	0.0373(3)
Si2	0.79106(12)	0.51775(10)	0.74749(9)	0.0258(3)
O1	0.6338(3)	0.5432(3)	0.7142(3)	0.0346(8)
C2	0.7815(4)	0.4467(4)	0.8579(3)	0.0220(9)
C3	0.8259(4)	0.3280(4)	0.8477(3)	0.0223(9)
C4	0.9636(4)	0.3139(4)	0.8728(3)	0.0264(9)
C5	0.9993(5)	0.2034(4)	0.8636(3)	0.0310(10)
C6	0.9001(5)	0.1029(4)	0.8315(4)	0.0344(11)
C7	0.7644(5)	0.1133(4)	0.8058(3)	0.0297(10)
C8	0.7275(4)	0.2249(4)	0.8137(3)	0.0235(9)
C9	0.4322(4)	0.1400(4)	0.8120(3)	0.0255(9)
C10	0.4413(5)	0.1149(5)	0.9060(4)	0.0402(12)
C11	0.3428(6)	0.0310(6)	0.9270(5)	0.0478(14)
C12	0.2354(5)	0.9713(5)	0.8551(4)	0.0400(12)
C13	0.2249(5)	0.9950(4)	0.7620(4)	0.0358(11)
C14	0.3227(5)	0.0799(4)	0.7405(4)	0.0296(10)
C15	0.5206(4)	0.2405(4)	0.6545(3)	0.0238(9)
C16	0.5832(5)	0.1595(4)	0.5907(3)	0.0298(10)
C17	0.5575(6)	0.1439(5)	0.4874(4)	0.0431(13)
C18	0.4710(7)	0.2088(6)	0.4486(4)	0.0527(16)
C19	0.4108(6)	0.2904(5)	0.5101(4)	0.0440(13)
C20	0.4320(5)	0.3081(4)	0.6151(4)	0.0316(10)
C21	0.3672(5)	0.3975(4)	0.6807(4)	0.0395(12)
C22A	0.4265(11)	0.6453(10)	0.8327(8)	0.031(2)
C23A	0.3011(11)	0.6322(10)	0.8899(8)	0.026(2)
C24A	0.3866(15)	0.6953(12)	0.7415(8)	0.057(3)
C25A	0.896(2)	0.6673(16)	0.7960(12)	0.029(3)
C26A	0.8341(14)	0.7471(11)	0.8780(9)	0.034(2)
C27A	0.915(4)	0.726(3)	0.7077(14)	0.035(4)

	x/a	y/b	z/c	U(eq)
C22B	0.4244(11)	0.6547(9)	0.7879(9)	0.029(2)
C24B	0.5286(10)	0.7684(7)	0.8266(7)	0.031(2)
C23B	0.3061(11)	0.6530(11)	0.8541(11)	0.030(3)
C25B	0.918(2)	0.6641(17)	0.7730(12)	0.026(3)
C26B	0.9015(15)	0.7418(11)	0.8745(9)	0.033(3)
C27B	0.903(4)	0.733(3)	0.6906(14)	0.036(4)
C28	0.8462(4)	0.4162(4)	0.6375(3)	0.0287(9)
C29	0.7912(5)	0.4336(5)	0.5354(3)	0.0401(11)
C30	0.0045(4)	0.4234(5)	0.6469(4)	0.0354(10)
C1S	0.0377(6)	0.9118(5)	0.4295(4)	0.0457(13)
C2S	0.1150(6)	0.0235(5)	0.4533(4)	0.0418(12)
C3S	0.0776(5)	0.1114(5)	0.5241(4)	0.0377(11)

Table S9*. Bond lengths (Å) for Cu_A_VM_005_bi.*

Rh1-C2	2.108(4)	Rh1-P1	2.2087(14)
Rh1-Si1	2.2663(18)	Rh1-Cl1	2.4167(15)
Rh1-Cl1	2.4460(16)	P1-C8	1.810(4)
P1-C9	1.821(5)	P1-C15	1.823(5)
Si1-O1	1.649(4)	Si1-C21	1.895(5)
Si1-C22A	1.897(11)	Si1-C22B	1.934(12)
Si2-O1	1.663(3)	Si2-C25A	1.87(2)
Si2-C28	1.886(5)	Si2-C2	1.900(5)
Si2-C25B	1.93(2)	C2-C3	1.507(6)
C2-H2	1.0	C3-C8	1.408(6)
C3-C4	1.411(6)	C4-C5	1.380(7)
C4-H4	0.95	C5-C6	1.390(7)
C5-H5	0.95	C6-C7	1.381(7)
C6-H6	0.95	C7-C8	1.399(7)
C7-H7	0.95	C9-C14	1.391(6)
C9-C10	1.393(7)	C10-C11	1.384(8)
C10-H10	0.95	C11-C12	1.379(9)
C11-H11	0.95	C12-C13	1.374(8)
C12-H12	0.95	C13-C14	1.391(7)
C13-H13	0.95	C14-H14	0.95
C15-C16	1.398(6)	C15-C20	1.413(7)

C16-C17	1.393(7)	C16-H16	0.95
C17-C18	1.372(9)	C17-H17	0.95
C18-C19	1.373(9)	C18-H18	0.95
C19-C20	1.410(7)	C19-H19	0.95
C20-C21	1.486(7)	C21-H21A	0.99
C21-H21B	0.99	C22A-C23A	1.531(9)
C22A-C24A	1.548(9)	C22A-H22A	1.0
C23A-H23A	0.98	C23A-H23B	0.98
C23A-H23C	0.98	C24A-H24A	0.98
C24A-H24B	0.98	C24A-H24C	0.98
C25A-C26A	1.533(9)	C25A-C27A	1.546(9)
C25A-H25A	1.0	C26A-H26A	0.98
C26A-H26B	0.98	C26A-H26C	0.98
C27A-H27A	0.98	C27A-H27B	0.98
C27A-H27C	0.98	C22B-C24B	1.532(9)
C22B-C23B	1.543(9)	C22B-H22B	1.0
C24B-H24D	0.98	C24B-H24E	0.98
C24B-H24F	0.98	C23B-H23D	0.98
C23B-H23E	0.98	C23B-H23F	0.98
C25B-C26B	1.531(9)	C25B-C27B	1.544(9)
C25B-H25B	1.0	C26B-H26D	0.98
C26B-H26E	0.98	C26B-H26F	0.98
C27B-H27D	0.98	C27B-H27E	0.98
C27B-H27F	0.98	C28-C29	1.532(6)
C28-C30	1.541(6)	C28-H28	1.0
C29-H29A	0.98	C29-H29B	0.98
C29-H29C	0.98	C30-H30A	0.98
C30-H30B	0.98	C30-H30C	0.98
C1S-C3S	1.375(8)	C1S-C2S	1.384(8)
C1S-H1S	0.95	C2S-C3S	1.374(7)
C2S-H2S	0.95	C3S-H3S	0.95

Table S10. ***Bond angles (°) for Cu_A_VM_005_bi***

C2-Rh1-P1	82.67(11)	C2-Rh1-Si1	92.45(13)
P1-Rh1-Si1	89.51(6)	C2-Rh1-Cl1	91.64(11)
P1-Rh1-Cl1	168.77(5)	Si1-Rh1-Cl1	100.44(7)
C2-Rh1-Cl1	169.88(13)	P1-Rh1-Cl1	97.46(5)
Si1-Rh1-Cl1	97.68(6)	Cl1-Rh1-Cl1	86.44(5)
Rh1-Cl1-Rh1	93.56(5)	C8-P1-C9	108.0(2)
C8-P1-C15	106.91(19)	C9-P1-C15	102.6(2)
C8-P1-Rh1	98.87(14)	C9-P1-Rh1	116.41(14)
C15-P1-Rh1	123.00(15)	O1-Si1-C21	108.1(2)
O1-Si1-C22A	112.2(3)	C21-Si1-C22A	112.2(4)
O1-Si1-C22B	99.7(3)	C21-Si1-C22B	104.2(4)
O1-Si1-Rh1	106.83(13)	C21-Si1-Rh1	109.76(19)
C22A-Si1-Rh1	107.7(3)	C22B-Si1-Rh1	126.8(4)
O1-Si2-C25A	104.5(6)	O1-Si2-C28	108.32(18)
C25A-Si2-C28	118.1(5)	O1-Si2-C2	107.84(18)
C25A-Si2-C2	106.7(6)	C28-Si2-C2	110.85(19)
O1-Si2-C25B	108.3(7)	C28-Si2-C25B	106.4(5)
C2-Si2-C25B	114.9(6)	Si1-O1-Si2	122.6(2)
C3-C2-Si2	118.0(3)	C3-C2-Rh1	107.0(3)
Si2-C2-Rh1	110.3(2)	C3-C2-H2	107.0
Si2-C2-H2	107.0	Rh1-C2-H2	107.0
C8-C3-C4	117.1(4)	C8-C3-C2	119.9(4)
C4-C3-C2	122.9(4)	C5-C4-C3	121.0(4)
C5-C4-H4	119.5	C3-C4-H4	119.5
C4-C5-C6	120.9(4)	C4-C5-H5	119.5
C6-C5-H5	119.5	C7-C6-C5	119.7(4)
C7-C6-H6	120.2	C5-C6-H6	120.2
C6-C7-C8	119.8(4)	C6-C7-H7	120.1
C8-C7-H7	120.1	C7-C8-C3	121.5(4)
C7-C8-P1	126.8(3)	C3-C8-P1	111.6(3)
C14-C9-C10	118.8(4)	C14-C9-P1	121.8(4)
C10-C9-P1	119.2(4)	C11-C10-C9	120.1(5)
C11-C10-H10	119.9	C9-C10-H10	119.9
C12-C11-C10	120.5(5)	C12-C11-H11	119.8
C10-C11-H11	119.8	C13-C12-C11	120.2(5)
C13-C12-H12	119.9	C11-C12-H12	119.9

C12-C13-C14	119.8(5)	C12-C13-H13	120.1
C14-C13-H13	120.1	C9-C14-C13	120.6(5)
C9-C14-H14	119.7	C13-C14-H14	119.7
C16-C15-C20	120.5(4)	C16-C15-P1	119.0(4)
C20-C15-P1	120.5(3)	C17-C16-C15	120.2(5)
C17-C16-H16	119.9	C15-C16-H16	119.9
C18-C17-C16	119.6(5)	C18-C17-H17	120.2
C16-C17-H17	120.2	C17-C18-C19	121.0(5)
C17-C18-H18	119.5	C19-C18-H18	119.5
C18-C19-C20	121.4(5)	C18-C19-H19	119.3
C20-C19-H19	119.3	C19-C20-C15	117.3(5)
C19-C20-C21	120.8(5)	C15-C20-C21	121.9(4)
C20-C21-Si1	111.9(3)	C20-C21-H21A	109.2
Si1-C21-H21A	109.2	C20-C21-H21B	109.2
Si1-C21-H21B	109.2	H21A-C21-H21B	107.9
C23A-C22A-C24A	108.8(7)	C23A-C22A-Si1	119.9(7)
C24A-C22A-Si1	102.3(7)	C23A-C22A-H22A	108.4
C24A-C22A-H22A	108.4	Si1-C22A-H22A	108.4
C22A-C23A-H23A	109.5	C22A-C23A-H23B	109.5
H23A-C23A-H23B	109.5	C22A-C23A-H23C	109.5
H23A-C23A-H23C	109.5	H23B-C23A-H23C	109.5
C22A-C24A-H24A	109.5	C22A-C24A-H24B	109.5
H24A-C24A-H24B	109.5	C22A-C24A-H24C	109.5
H24A-C24A-H24C	109.5	H24B-C24A-H24C	109.5
C26A-C25A-C27A	109.8(8)	C26A-C25A-Si2	113.9(11)
C27A-C25A-Si2	108.9(16)	C26A-C25A-H25A	108.0
C27A-C25A-H25A	108.0	Si2-C25A-H25A	108.0
C25A-C26A-H26A	109.5	C25A-C26A-H26B	109.5
H26A-C26A-H26B	109.5	C25A-C26A-H26C	109.5
H26A-C26A-H26C	109.5	H26B-C26A-H26C	109.5
C25A-C27A-H27A	109.5	C25A-C27A-H27B	109.5
H27A-C27A-H27B	109.5	C25A-C27A-H27C	109.5
H27A-C27A-H27C	109.5	H27B-C27A-H27C	109.5
C24B-C22B-C23B	110.1(8)	C24B-C22B-Si1	115.7(8)
C23B-C22B-Si1	110.3(7)	C24B-C22B-H22B	106.8
C23B-C22B-H22B	106.8	Si1-C22B-H22B	106.8
C22B-C24B-H24D	109.5	C22B-C24B-H24E	109.5

H24D-C24B-H24E	109.5	C22B-C24B-H24F	109.5
H24D-C24B-H24F	109.5	H24E-C24B-H24F	109.5
C22B-C23B-H23D	109.5	C22B-C23B-H23E	109.5
H23D-C23B-H23E	109.5	C22B-C23B-H23F	109.5
H23D-C23B-H23F	109.5	H23E-C23B-H23F	109.5
C26B-C25B-C27B	110.0(9)	C26B-C25B-Si2	109.9(11)
C27B-C25B-Si2	114.0(19)	C26B-C25B-H25B	107.5
C27B-C25B-H25B	107.5	Si2-C25B-H25B	107.5
C25B-C26B-H26D	109.5	C25B-C26B-H26E	109.5
H26D-C26B-H26E	109.5	C25B-C26B-H26F	109.5
H26D-C26B-H26F	109.5	H26E-C26B-H26F	109.5
C25B-C27B-H27D	109.5	C25B-C27B-H27E	109.5
H27D-C27B-H27E	109.5	C25B-C27B-H27F	109.5
H27D-C27B-H27F	109.5	H27E-C27B-H27F	109.5
C29-C28-C30	110.6(4)	C29-C28-Si2	114.2(3)
C30-C28-Si2	111.4(3)	C29-C28-H28	106.7
C30-C28-H28	106.7	Si2-C28-H28	106.7
C28-C29-H29A	109.5	C28-C29-H29B	109.5
H29A-C29-H29B	109.5	C28-C29-H29C	109.5
H29A-C29-H29C	109.5	H29B-C29-H29C	109.5
C28-C30-H30A	109.5	C28-C30-H30B	109.5
H30A-C30-H30B	109.5	C28-C30-H30C	109.5
H30A-C30-H30C	109.5	H30B-C30-H30C	109.5
C3S-C1S-C2S	120.1(5)	C3S-C1S-H1S	119.9
C2S-C1S-H1S	119.9	C3S-C2S-C1S	120.1(5)
C3S-C2S-H2S	119.9	C1S-C2S-H2S	119.9
C2S-C3S-C1S	119.7(5)	C2S-C3S-H3S	120.1
C1S-C3S-H3S	120.1		

4 Computational details

The minimum and transition states were located on Gaussian 16 software[17] with ωB97XD[18-19] functional theory. In terms of basis set (BS1), 6-31G(d')[20-22] was used for H and C; LanL2DZ(d,p)[23-25] and associated ECP was used for P, Si and Cl; and SDD (as defined in the G16 code) for Rh.[26] Frequency calculations were performed to obtain thermodynamic and kinetic values and to ensure that minima and transition states have zero and one imaginary frequency, respectively.

The geometries associated with the displacement of atoms along imaginary frequencies in the transition states were also located to verify the appropriate connected minima. Solvent effects also are included via single-point calculations utilizing gas-phase geometries with the SMD implicit solvation model.[27]

For the thermodynamic calculation of the monomer-dimer equilibria, a single-point calculation was performed using the ωB97XD functional and the BS2 basis set. The optimized geometries of the complexes were used as input for these calculations. In the BS2 basis set, 6-311+G(2d,p) basis set is applied for C, H, P, Si, Cl atoms and SDD pseudo potential for Rh. The results for the monomer-dimer equilibria in Scheme 3 in the main text were reported at the ωB97XD/BS2//BS1 level of theory.

Mechanistic possibilities

The formation of the isomerized product **Rh-3** was explored from two starting materials: (1) $[RhCl(COD)]_2$ dimer and (2) **Rh-1**. In accordance with the experiment, the formation of **Rh-3** is more favorable to occur during the metalation process, e.g. directly from $[RhCl(COD)]_2$.

Mechanism of formation of Rh-3 from $[RhCl(COD)]_2$

We propose a mechanism consisting of two main parts. Firstly, the formation of intermediate **Rh-8** occurs during metalation (**Figure S8**). From this intermediate, two competitive pathways arise, leading to the formation of **Rh-1** and its isomer, **Rh-3-mon**.

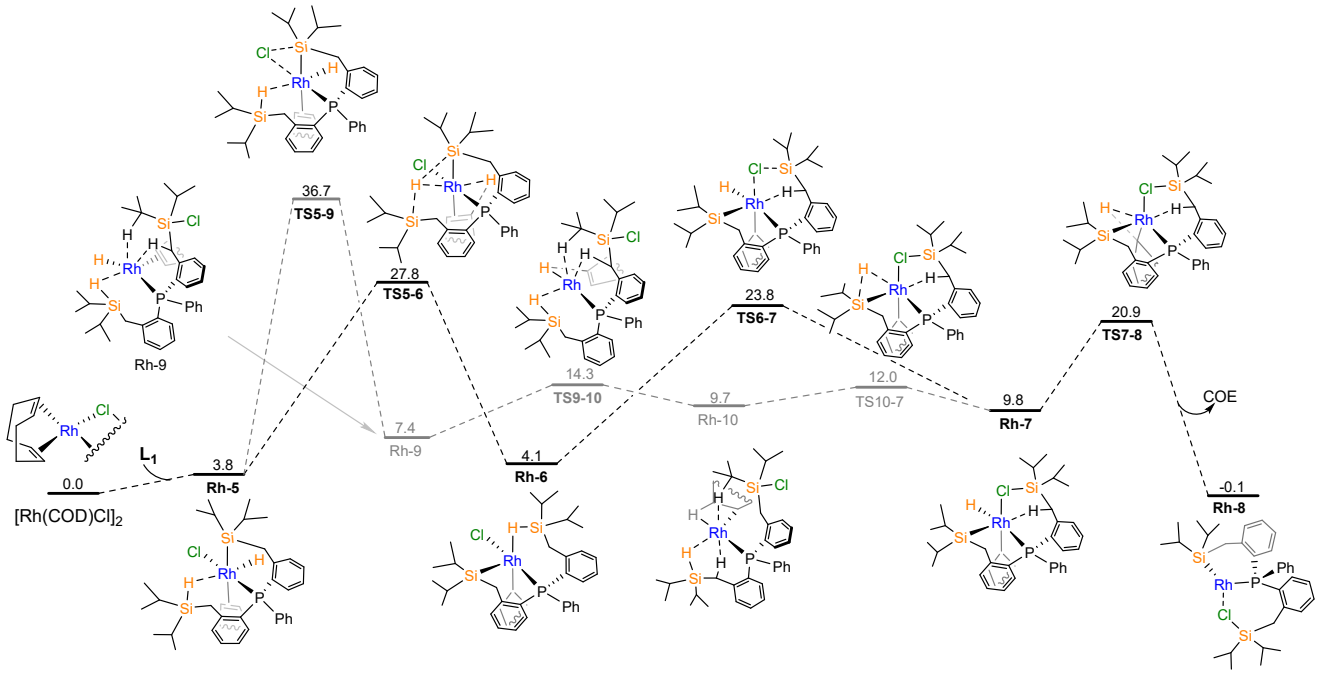

Figure S8. Gibbs free energy diagram at SMD(benzene)-ωB97XD//ωB97XD/BS1 level theory producing intermediate **Rh-8**

Mechanism of formation of Rh-3 from Rh-1

To study the isomerization process, at first, three possible paths were explored in the starting 14e$^-$ species **Rh-1**, see Figure S9. In this discussion, **Rh-1** is used as the reference energy point at 0.0 kcal/mol. Two σ-bond metathesis (SM) processes attempting to make Rh-C bond directly requires significant energy at **TS1-18**, $\Delta^{\ddagger}G°$=53.5 kcal/mol and **TS1-19**, $\Delta^{\ddagger}G°$=40.9 kcal/mol (Figure S9). A silylene intermediate is also proposed as this intermediate would result from C-C bond cleavage, but the geometry could not be located. The only viable energy pathway that was found is the reductive elimination (RE) step, **TS1-8**, $\Delta^{\ddagger}G°$=26.2 kcal/mol, which potentially initiates the isomerization process.

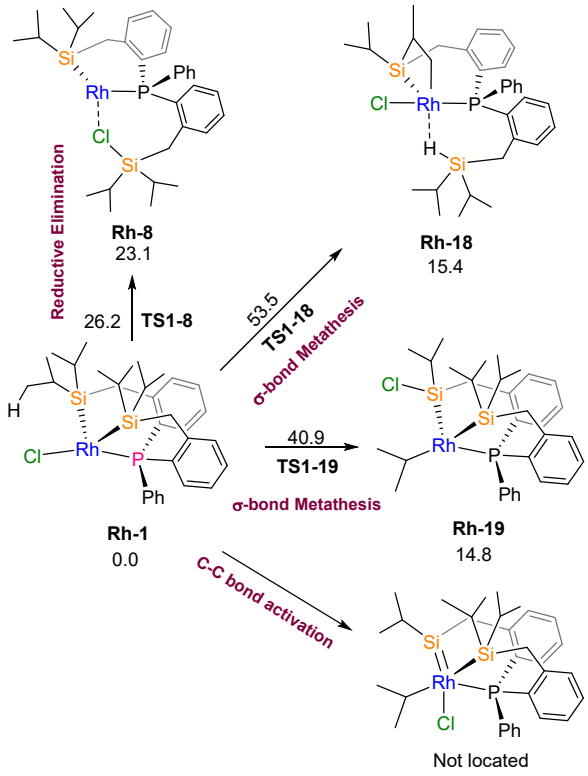

Figure S9. Exploring the reactivity of complex **Rh-1**. Calculated at ωB97XD/BS1 level theory

The present study elucidates the transformation from an isopropyl silyl complex to a terminal *n*-propyl species, which can be summarized in six steps: reductive elimination (RE), oxidative addition (OA), σ-bond metathesis (SM), σ-bond metathesis (SM), reductive elimination (RE), and oxidative addition (OA), as illustrated in Figure S10. Following the first reductive elimination (RE) step, a Si-Cl bond is formed in the **Rh-8** complex, while Cl continues to serve as a ligand in the $14e^-$ Rhodium(I) complex. There is another isomer in which an agostic interaction replaces the coordination of chlorine. This isomer, denoted as **Rh-11**, has a slightly higher energy of 1.1 kcal/mol compared to −0.1 kcal/mol in **Rh-8**.

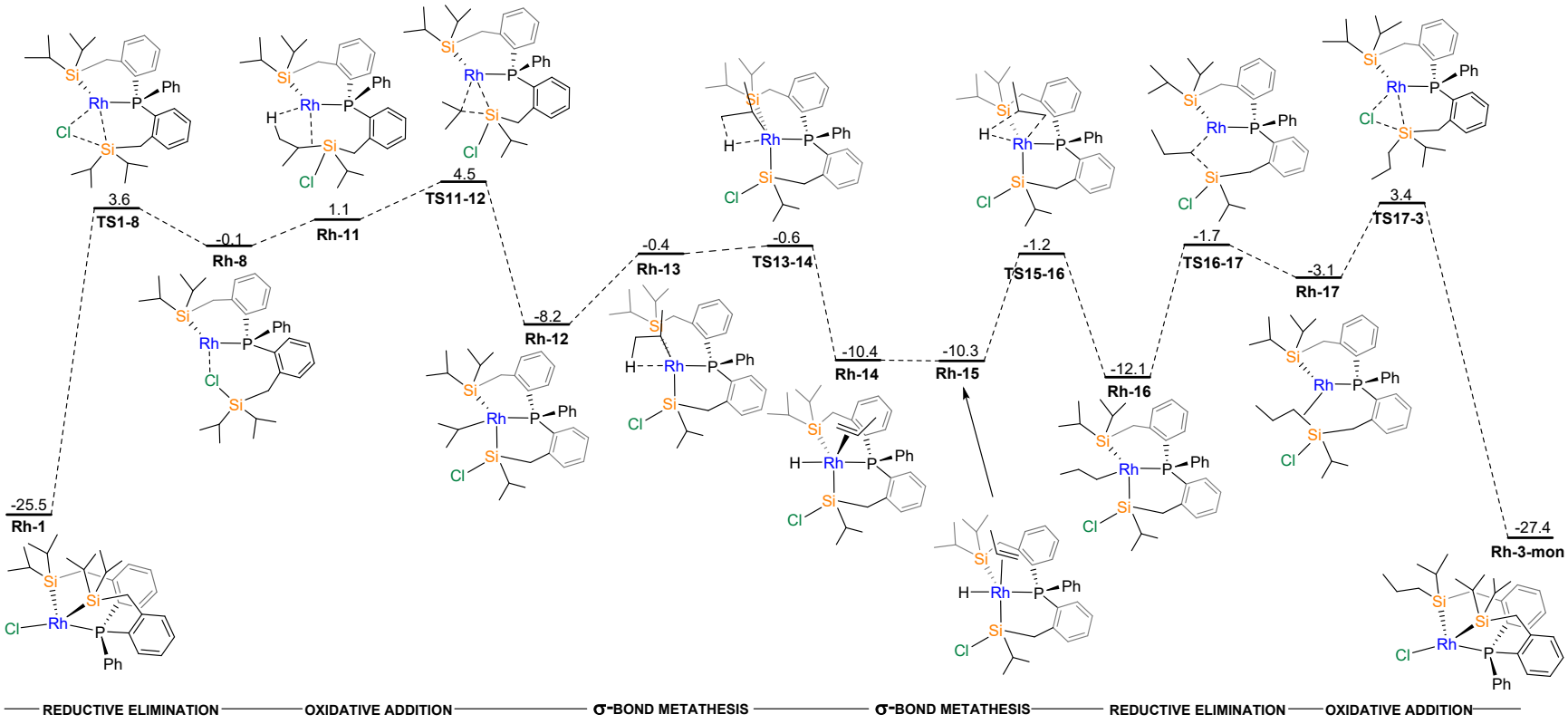

Figure S10. Gibbs free energy diagram (kcal/mol) for the isomerization process at SMD(benzene)-ωB97XD//ωB97XD/BS1 level theory.

This species with an agostic interaction accommodates the proper proximality to break the C-Si bond at **TS11-12** which is the rate determining step with $\Delta\Delta^{\ddagger}G°$=30.0 kcal/mol (energy gap between **TS11-12** and **Rh-1**). In this point, breaking the C-Si bond produces **Rh-12** where the Rh(III) center bonds to the isopropyl group. Next, a couple of *σ*-bond metathesis steps occur which isomerize the isopropyl ligand to the terminal propyl ligand. A β-hydride elimination step **TS13-14,** $\Delta^{\ddagger}G°$=–0.6 kcal/mol produces trigonal pyramidal hydride complex **Rh-14** followed by the conformer change on the alkene ligand which leads to minimum **Rh-15**. Then, the hydride returns to the alkyl chain via another *σ*-bond metathesis event, **TS15-16**, $\Delta^{\ddagger}G°$=–1.2 kcal/mol. The analogous metathesis computations performed on different isomers where the hydride and alkene ligand switch positions (the hydride is no longer located in the trans position to the phosphine ligand but instead to the alkene ligand) show a less favorable free energy of activation, see Figure S11.

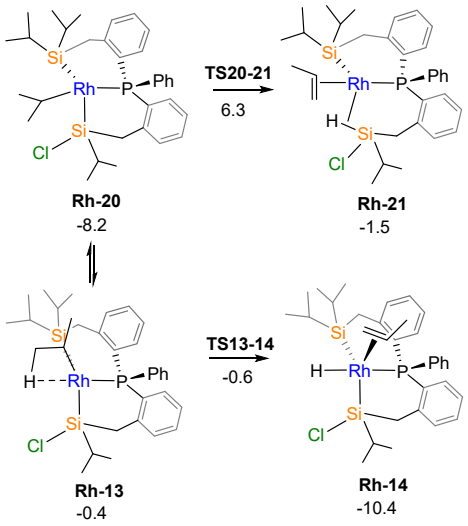

Figure S11. Energy comparison of *σ*-bond metathesis between two different isomers. Calculated at SMD(benzene)-ωB97XD//ωB97XD/BS1 level theory.

The relative energy of complex **Rh-17** is comparable to that of complex **Rh-8**, and the transformation of complex **Rh-17** to **Rh-3-mon** follows an analogous reverse pathway to that of the transformation from complex **Rh-1** to **Rh-8**. Typically, intermediates with terminal alkyl ligands exhibit slightly lower thermodynamic stability compared to those with branched alkyl ligands. As a result, the isomerization process is thermodynamically favorable, with an approximate energy difference of −1.9 kcal/mol.

Table S11. Selected relative free Gibbs energy (kcal/mol) comparison between ωB97XD/BS1 and SMD(benzene)-ωB97XD//ωB97XD/BS1 level theory.

Complexes	ωB97XD/BS1	SMD(Benzene)-ωB97XD//ωB97XD/BS1
$[Rh(COD)Cl]_2$	0.0	0.0
Rh-1	-23.5	-25.5
Rh-3-mon	-25.7	-27.4
Rh-5	2.4	3.8
Rh-6	3.9	4.1
Rh-7	7.9	9.8
Rh-8	-0.4	-0.1
TS5-6	25.3	27.8
TS6-7	20.2	23.8
TS7-8	20.3	20.9
TS1-8	2.7	3.6
TS11-12	4.9	4.5

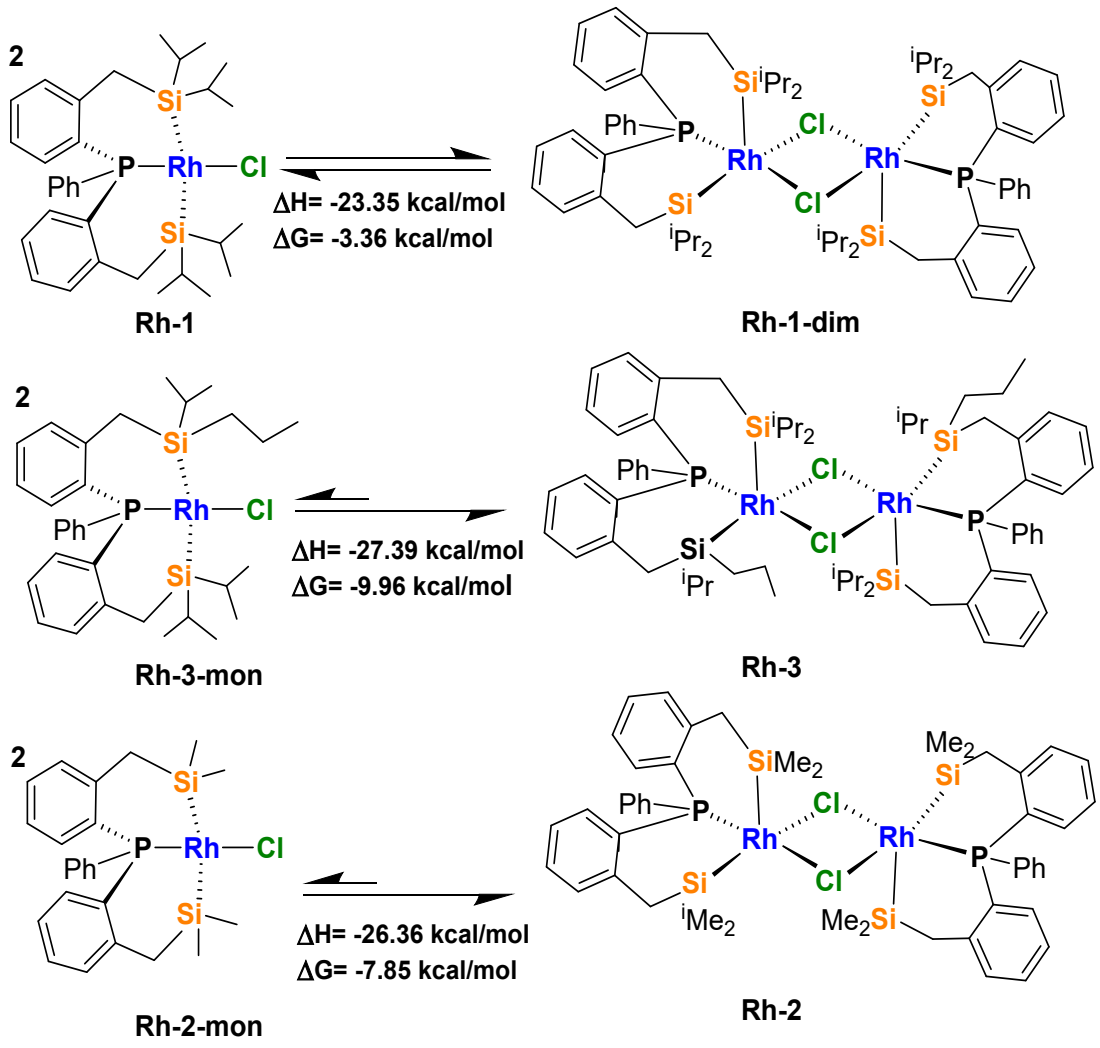

Figure S12. The monomer/dimer equilibria upon variation of the substituents on Si in (κ3-Si,Si,P)RhCl complexes and the calculated energetic parameters (at the ωB97XD/BS1 level of theory).

5 References

1. Giordano, G.; Crabtree, R. H.; Heintz, R. M.; Forster, D.; Morris, D. E., Di-μ-Chloro-Bis(η4-1,5-Cyclooctadlene) Dirhodium(I). In *Inorg. Synth.*, John Wiley & Sons, Inc.: 2007; pp 218-220.
2. Corona-González, M. V.; Zamora-Moreno, J.; Muñoz-Hernández, M. A.; Vendier, L.; Sabo-Etienne, S.; Montiel-Palma, V., Exploiting the Versatility of Phosphinobenzylsilanes for the Stabilization of 14-Electron Rhodium(III) and Iridium(III) Complexes. *European Journal of Inorganic Chemistry* **2019,** *2019* (13), 1854-1858.
3. Corey, J. Y., Reactions of Hydrosilanes with Transition Metal Complexes. *Chem. Rev.* **2016,** *116* (19), 11291-11435.
4. Corey, J. Y.; Braddock-Wilking, J., Reactions of Hydrosilanes with Transition-Metal Complexes: Formation of Stable Transition-Metal Silyl Compounds. *Chem. Rev.* **1999,** *99* (1), 175-292.
5. Corey, J. Y., Reactions of Hydrosilanes with Transition Metal Complexes and Characterization of the Products. *Chem. Rev.* **2011,** *111* (2), 863-1071.
6. Pham, E. K.; West, R., Platinum .eta.2-disilene complexes: syntheses, reactivity, and structures. *Organometallics* **1990,** *9* (5), 1517-1523.
7. Noda, H.; Tanaka, K.; Tanabe, M.; Osakada, K., Cyclic Platina(borasiloxane)s and Platina(siloxane)s and Their Chemical Properties. *Organometallics* **2018,** *37* (1), 22-29.
8. DeMott, J. C.; Gu, W.; McCulloch, B. J.; Herbert, D. E.; Goshert, M. D.; Walensky, J. R.; Zhou, J.; Ozerov, O. V., Silyl–Silylene Interplay in Cationic PSiP Pincer Complexes of Platinum. *Organometallics* **2015,** *34* (16), 3930-3933.
9. Korshin, E. E.; Leitus, G.; Shimon, L. J. W.; Konstantinovski, L.; Milstein, D., Silanol-Based Pincer Pt(II) Complexes: Synthesis, Structure, and Unusual Reactivity. *Inorganic Chemistry* **2008,** *47* (16), 7177-7189.
10. Feldman, J. D.; Peters, J. C.; Tilley, T. D., Activations of Silanes with [PhB(CH2PPh2)3]Ir(H)(η3-C8H13). Formation of Iridium Silylene Complexes via the Extrusion of Silylenes from Secondary Silanes R2SiH2. *Organometallics* **2002,** *21* (20), 4065-4075.
11. Corona-Gonzalez, M. V.; Zamora-Moreno, J.; Cuevas-Chavez, C. A.; Rufino-Felipe, E.; Mothes-Martin, E.; Coppel, Y.; Munoz-Hernandez, M. A.; Vendier, L.; Flores-Alamo, M.; Grellier, M.; Sabo-Etienne, S.; Montiel-Palma, V., A family of rhodium and iridium complexes with semirigid benzylsilyl phosphines: from bidentate to tetradentate coordination modes. *Dalton Trans.* **2017,** *46* (27), 8827-8838.
12. Saint Program included in the package software: APEX4 v2021.4-0
13. Bruker (2001). Bruker AXS Inc., Madison, Wisconsin, USA.
14. SHELXT-Integrated space group and crystal -structure determination Sheldrick, G. M. Acta Crystallogr., Sect. A 2015, A71, 3-8.
15. SHELXT Sheldrick, G. M. Ver. 2018/3. Acta Crystallogr. Sect. C Structural Chemistry 71, 3-8.
16. APEX4 v2021, 4-0, AXS Bruker program.
17. Frisch, M. J.; Trucks, G. W.; Schlegel, H. B.; Scuseria, G. E.; Robb, M. A.; Cheeseman, J. R.; Scalmani, G.; Barone, V.; Petersson, G. A.; Nakatsuji, H.; Li, X.; Caricato, M.; Marenich, A. V.; Bloino, J.; Janesko, B. G.; Gomperts, R.; Mennucci, B.; Hratchian, H. P.; Ortiz, J. V.; Izmaylov, A. F.; Sonnenberg, J. L.; Williams; Ding, F.; Lipparini, F.; Egidi, F.; Goings, J.; Peng, B.; Petrone, A.; Henderson, T.; Ranasinghe, D.; Zakrzewski, V. G.; Gao, J.; Rega, N.; Zheng, G.; Liang, W.; Hada, M.; Ehara, M.; Toyota, K.; Fukuda, R.; Hasegawa, J.; Ishida, M.; Nakajima, T.; Honda, Y.; Kitao, O.; Nakai, H.; Vreven, T.; Throssell, K.; Montgomery Jr., J. A.; Peralta, J. E.; Ogliaro, F.; Bearpark, M. J.; Heyd, J. J.; Brothers, E. N.; Kudin, K. N.; Staroverov, V. N.; Keith, T. A.; Kobayashi, R.; Normand, J.; Raghavachari, K.; Rendell, A. P.; Burant, J. C.; Iyengar, S. S.; Tomasi, J.; Cossi, M.; Millam, J. M.; Klene, M.; Adamo, C.; Cammi, R.; Ochterski, J. W.;

Martin, R. L.; Morokuma, K.; Farkas, O.; Foresman, J. B.; Fox, D. J. *Gaussian 16 Rev. C.01*, Wallingford, CT, 2016.
18. Chai, J. D.; Head-Gordon, M., Long-range corrected hybrid density functionals with damped atom-atom dispersion corrections. *PCCP* **2008,** *10* (44), 6615-20.
19. Chai, J. D.; Head-Gordon, M., Systematic optimization of long-range corrected hybrid density functionals. *The Journal of Chemical Physics* **2008,** *128* (8), 084106.
20. Hehre, W. J.; Ditchfield, R.; Pople, J. A., Self—Consistent Molecular Orbital Methods. XII. Further Extensions of Gaussian—Type Basis Sets for Use in Molecular Orbital Studies of Organic Molecules. *The Journal of Chemical Physics* **1972,** *56* (5), 2257-2261.
21. Hariharan, P. C.; Pople, J. A., The influence of polarization functions on molecular orbital hydrogenation energies. *Theoretica chimica acta* **1973,** *28* (3), 213-222.
22. Petersson, G. A.; Al-Laham, M. A., A complete basis set model chemistry. II. Open-shell systems and the total energies of the first-row atoms. *The Journal of Chemical Physics* **1991,** *94* (9), 6081-6090.
23. Hay, P. J.; Wadt, W. R., Ab initio effective core potentials for molecular calculations. Potentials for K to Au including the outermost core orbitals. *The Journal of Chemical Physics* **1985,** *82* (1), 299-310.
24. Hay, P. J.; Wadt, W. R., Ab initio effective core potentials for molecular calculations. Potentials for the transition metal atoms Sc to Hg. *The Journal of Chemical Physics* **1985,** *82* (1), 270-283.
25. Couty, M.; Hall, M. B., Basis sets for transition metals: Optimized outer p functions. *Journal of Computational Chemistry* **1996,** *17* (11), 1359-1370.
26. Andrae, D.; Häußermann, U.; Dolg, M.; Stoll, H.; Preuß, H., Energy-adjustedab initio pseudopotentials for the second and third row transition elements. *Theoretica chimica acta* **1990,** *77* (2), 123-141.
27. Marenich, A. V.; Cramer, C. J.; Truhlar, D. G., Universal Solvation Model Based on Solute Electron Density and on a Continuum Model of the Solvent Defined by the Bulk Dielectric Constant and Atomic Surface Tensions. *The Journal of Physical Chemistry B* **2009,** *113* (18), 6378-6396.